Journal of Hydrology 540 (2016) 914–922

Contents lists available at ScienceDirect

Journal of Hydrology

journal homepage: www.elsevier.com/locate/jhydrol

Research papers

Testing the generalized complementary relationship of evaporation with continental-scale long-term water-balance data

Jozsef Szilagyi [a,b,*], Richard Crago [c], Russell J. Qualls [d]

[a] School of Natural Resources, Conservation and Survey Division, University of Nebraska-Lincoln, Lincoln, NE 68583, USA
[b] Department of Hydraulic and Water Resources Engineering, Budapest University of Technology and Economics, Muegyetem Rakpart. 3–9, 1111 Budapest, Hungary
[c] Department of Civil and Environmental Engineering, Bucknell University, Lewisburg, PA 17837, USA
[d] Department of Biological Engineering, University of Idaho, Moscow, ID 83844, USA

ARTICLE INFO

Article history:
Received 8 March 2016
Received in revised form 18 May 2016
Accepted 1 July 2016
Available online 2 July 2016
This manuscript was handled by Tim R. McVicar, Editor-in-Chief, with the assistance of Dawen Yang, Associate Editor

Keywords:
Complementary relationship
Evaporation
Water balance

ABSTRACT

The original and revised versions of the generalized complementary relationship (GCR) of evaporation (*ET*) were tested with six-digit Hydrologic Unit Code (HUC6) level long-term (1981–2010) water-balance data (sample size of 334). The two versions of the GCR were calibrated with Parameter-Elevation Regressions on Independent Slopes Model (PRISM) mean annual precipitation (*P*) data and validated against water-balance ET (ET_{wb}) as the difference of mean annual HUC6-averaged *P* and United States Geological Survey HUC6 runoff (*Q*) rates. The original GCR overestimates *P* in about 18% of the PRISM grid points covering the contiguous United States in contrast with 12% of the revised version. With HUC6-averaged data the original version has a bias of -25 mm yr^{-1} vs the revised version's -17 mm yr^{-1}, and it tends to more significantly underestimate ET_{wb} at high values than the revised one (slope of the best fit line is 0.78 vs 0.91). At the same time it slightly outperforms the revised version in terms of the linear correlation coefficient (0.94 vs 0.93) and the root-mean-square error (90 vs 92 mm yr^{-1}).

1. Introduction

The Complementary Relationship (CR) of evaporation (Bouchet, 1963) is a physically based approach that yields actual evapotranspiration rates (*ET*) without detailed knowledge of the land-surface properties: terrain, land-cover and soil type, as well as soil-moisture status. This makes the CR undeniably appealing. The CR implicitly accounts for the complex interplay between the land, vegetation, and atmospheric components by relating the typically moisture-limited actual *ET* to two energy-limited evaporation rates of fully wet surfaces differing mostly in horizontal extent: one from a small wet patch or a shallow pond or even an evaporation pan (E_p in mm d^{-1}) under the prevailing atmospheric conditions, the other, from a wet landscape (E_w in mm d^{-1}), driven predominantly by the available energy (R_n) at the surface (Priestley and Taylor, 1972)

$$E_w = \alpha \frac{\Delta(T_w)}{\Delta(T_w)+\gamma} R_n. \quad (1)$$

Here R_n is specified in water depth per unit time (mm d^{-1}), Δ (hPa K^{-1}) is the slope of the saturation vapor pressure curve at the wet environment air temperature, T_w (K), and γ [$= c_p p/(0.622L)$ in hPa K^{-1}] is the psychrometric constant, where c_p (J kg^{-1} K^{-1}) is the specific heat of air at constant pressure, p (hPa), and L (J kg^{-1}) is latent heat of vaporization for water. The dimensionless coefficient α (>1) is generally accepted to express the evaporation-enhancing effect of large-scale entrainment of drier free-tropospheric air resulting from the growing daytime convective boundary layer (Brutsaert, 1982; de Bruin, 1983; Culf, 1994; Lhomme, 1997; Heerwaarden et al., 2009). T_w can be estimated from the prevailing air temperature, T_a (K) via an implicit formula based on the Bowen ratio (B_o) written for a small wet surface with daily sums of the fluxes (Szilagyi and Jozsa, 2008) as

$$B_o \approx \frac{R_n - E_p}{E_p} \approx \gamma \frac{T_{ws} - T_a}{e*(T_{ws}) - e(T_a)} \quad (2)$$

making use of the assumption that R_n, T_a and the actual vapor pressure measurements, e (hPa), (e^* its saturated value) are also valid over the wet surface due to the small extent of the latter. T_{ws} (K) is the estimated air temperature at the wet surface, which has been shown to be independent of the horizontal extent (Szilagyi and Schepers, 2014) of the wet patch. Since the equilibrium air

* Corresponding author at: School of Natural Resources, Conservation and Survey Division, University of Nebraska-Lincoln, Lincoln, NE 68583, USA.
E-mail address: jszilagyi1@unl.edu (J. Szilagyi).

http://dx.doi.org/10.1016/j.jhydrol.2016.07.001
0022-1694/

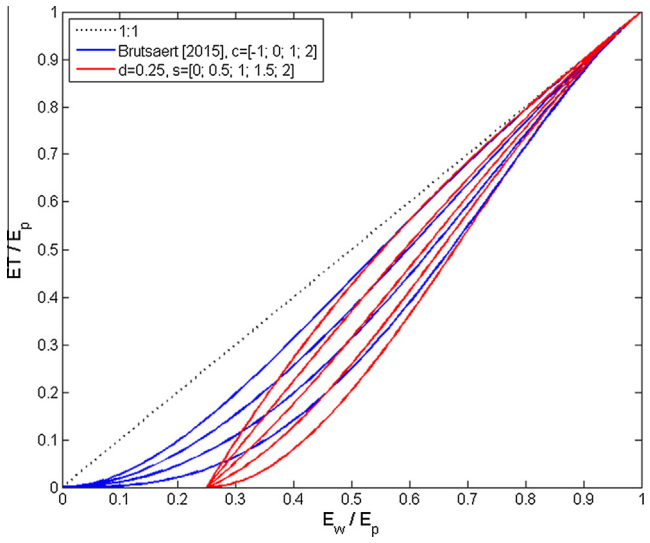

Fig. 1. Theory-predicted E_p-scaled evaporation rates for selected values of the parameters within the physically meaningful ranges of $-1 \leqslant c \leqslant 2$ for (8) and $0 \leqslant d < 1$, $0 \leqslant s \leqslant (2d+1)/(1-d)$ for (9) where thus $ET/E_p \leqslant E_w/E_p$ and ET/E_p monotonically increases with E_w/E_p. The two-parameter curve is valid for $E_w/E_p \geqslant d$ only. Parameter values of c decrease, while those of s increase from bottom to top of the corresponding series of curves.

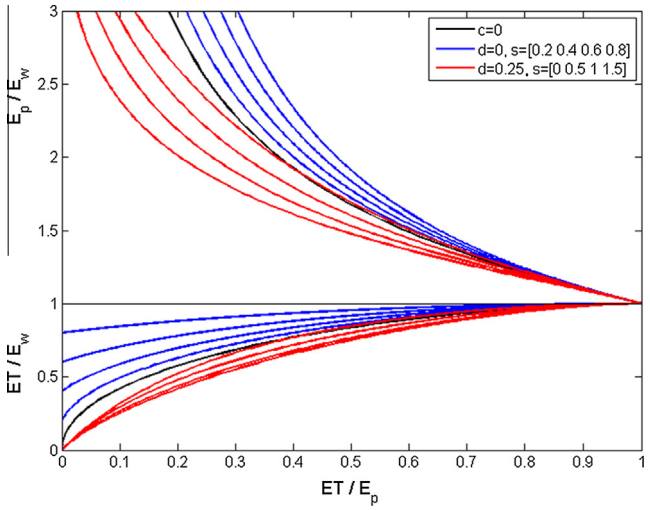

Fig. 2. Theory-predicted E_w-scaled actual and apparent potential evaporation rates for selected values of the parameters as a function of the moisture index, ET/E_p. The values of s increase from bottom to top of the corresponding series of curves.

temperature profile over an extended wet surface has a mild gradient with height above the ground (Szilagyi and Jozsa, 2009), the T_{ws} value estimated from (2) can be taken for T_w in (1) as long as $T_{ws} < T_a$, otherwise T_w can be replaced by T_a (Huntington et al., 2011; McMahon et al., 2013a, 2013b; Szilagyi, 2014a).

In lieu of direct measurements, the so-called apparent potential (Brutsaert, 2005) evaporation rate of the small wet surface can be defined by the Penman (1948) equation

$$E_p = \frac{\Delta(T_a)}{\Delta(T_a)+\gamma} R_n + \frac{\gamma}{\Delta(T_a)+\gamma} f_u [e*(T_a) - e(T_a)] \quad (3)$$

where f_u (mm d^{-1} hPa^{-1}) is an empirical wind function. With the proper choice of f_u, (3) can estimate E_p rates of a small pond, a wet patch or a sunken evaporation pan, i.e.,

$$f_u = 0.26(1 + 0.54u_2) \quad (4)$$

where u_2 is the wind speed (m s^{-1}) at 2 m above the ground (Brutsaert, 1982). As an alternative, monthly E_p rates of class-A evaporation pans can, however, be better estimated by a more sensitive f_u (Szilagyi and Jozsa, 2008)

$$f_u = 0.49(1 + 0.35u_2). \quad (5)$$

The difference in the two energy-limited evaporation rates, i.e., E_w and E_p, is due mainly to edge-effects: the horizontal energy transport [expressed by the second term of (3)] which is significant over the small, freely evaporating wet surface dissipates with the extent of the wet area. The more significant this edge effect, the more arid the environment has become, which forms the basis of the CR, typically written as

$$ET = E_w - (E_P - E_w)/b \quad (6)$$

where b^{-1} (–) (or b itself) is a proportionality coefficient (Kahler and Brutsaert, 2006; Szilagyi, 2007; Zuo et al., 2015). Kahler and Brutsaert (2006) assumed it to be a constant, i.e., $b = 4.5$, when employing class-A evaporation pans for obtaining E_p. The CR with the so-called Rome wind-function of (4) is typically found to be symmetric, i.e., $b = 1$ (Ramirez et al., 2005). Recently Szilagyi (2015) related b^{-1} to the relative humidity of the air via a modified logistic curve, using (5). Note that the three evaporation rates collapse into one under energy-limited conditions, i.e., $ET = E_w = E_p$.

An exciting new generalization of the CR has been developed recently by Brutsaert (2015) who originally spearheaded the employment of the complementary relationship for practical applications (Brutsaert and Stricker, 1979). The objectives of this study are (i) to introduce a revision to this newly generalized CR; and (ii) to compare the performance of the two versions via calibration with precipitation and validation against long-term (1981–2010) water-balance derived mean annual evaporation rates across the conterminous United States.

2. Theoretical background: The generalized complementary relationship (GCR)

Brutsaert (2015) reformulated the CR by setting physical constraints for the relationship between E_p-scaled actual ($y = ET/E_p$) and wet environment evaporations ($x = E_w/E_p$) in the form of boundary conditions (BC), inspired by the work of Han et al. (2012). The four BCs he employed for an assumed polynomial relationship between y and x are

$$\text{(i) } y = 1 \text{ at } x = 1; \text{(ii) } y = 0 \text{ at } x = 0; \text{(iii) } dy/dx = 1 \text{ at } x = 1; \text{(iv) } dy/dx = 0 \text{ at } x = 0. \quad (7)$$

BC (i) results from $ET = E_w = E_p$ under energy-limited conditions. BC (iii) is consistent with E_p values that are more sensitive to changes in moisture availability than ET itself, as x approaches unity. Brutsaert (2015) also introduced an additional parameter c (–) into the BC-derived polynomial relationship for added flexibility. The resulting relationship has become

$$y = (2-c)x^2 - (1-2c)x^3 - cx^4 \quad (8)$$

3. Methods

3.1. Revision of the GCR

(8) must satisfy two additional constraints (a) y must be monotonically increasing with respect to x; and (b) $y \leqslant x$ for $0 \leqslant x \leqslant 1$. These latter two conditions restrain the admissible range of c to $-1 \leqslant c \leqslant 2$, which is important to define for practical applications

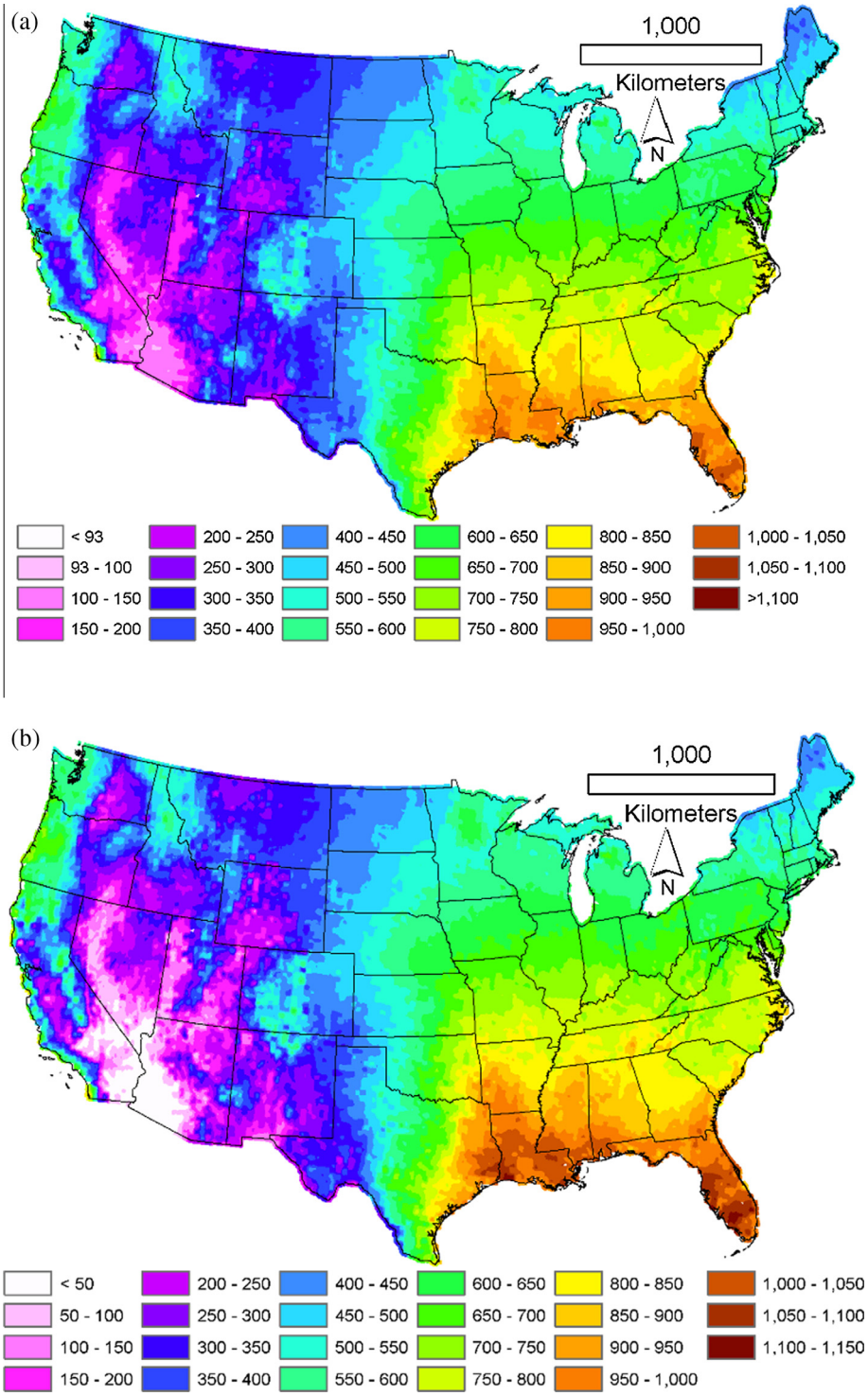

Fig. 3. Spatial distribution of the mean annual (1981–2010) *ET* rates estimated by (a) (8) with $\alpha = 1.09$ and $c = 2$ (sample mean with the standard deviation and extrema are: $\langle ET \rangle = 523 \pm 196$, $ET_{min} = 93$, $ET_{max} = 1055$, all in mm yr^{-1}); (b) (9) with $\alpha = 1.14$, d = 0.28, $s = 0$ ($\langle ET \rangle = 525 \pm 232$, $ET_{min} = 1$, $ET_{max} = 1130$, all in mm yr^{-1}).

where the value of c may be automatically calibrated. BCs (ii) and (iv) are a bit problematic because in an environment with no moisture availability *ET* can clearly be zero (thus y too) for $E_w > 0$ and therefore $x > 0$ since E_p is bounded by the physically possible wind speed and the moisture-holding capacity of the air (i.e. E_p cannot approach infinity to result in $x = 0$ for $E_w > 0$). Consequently these BCs are relaxed.

As y may reach zero for $x = d$, where $d > 0$, BC (ii) can be replaced by (ii)* $y = 0$ at $x = d$.

(Note that for the symmetric CR of Brutsaert and Stricker (1979) d is 0.5 when $y = 0$ and $dy/dx = 2$ at $x = d$) The new BC, (ii)*, has an effect on the slope (s) of y which may then be larger than zero at d. Thus (iv)* $dy/dx = s$ at $x = d$, with $s \geqslant 0$. With these two new (starred) BCs replacing the old ones, (ii) and (iv), the solution of the system of linear equations the BCs constitute for the unknown polynomial coefficients in

$$y = a_3x^3 + a_2x^2 + a_1x + a_0 \tag{9a}$$

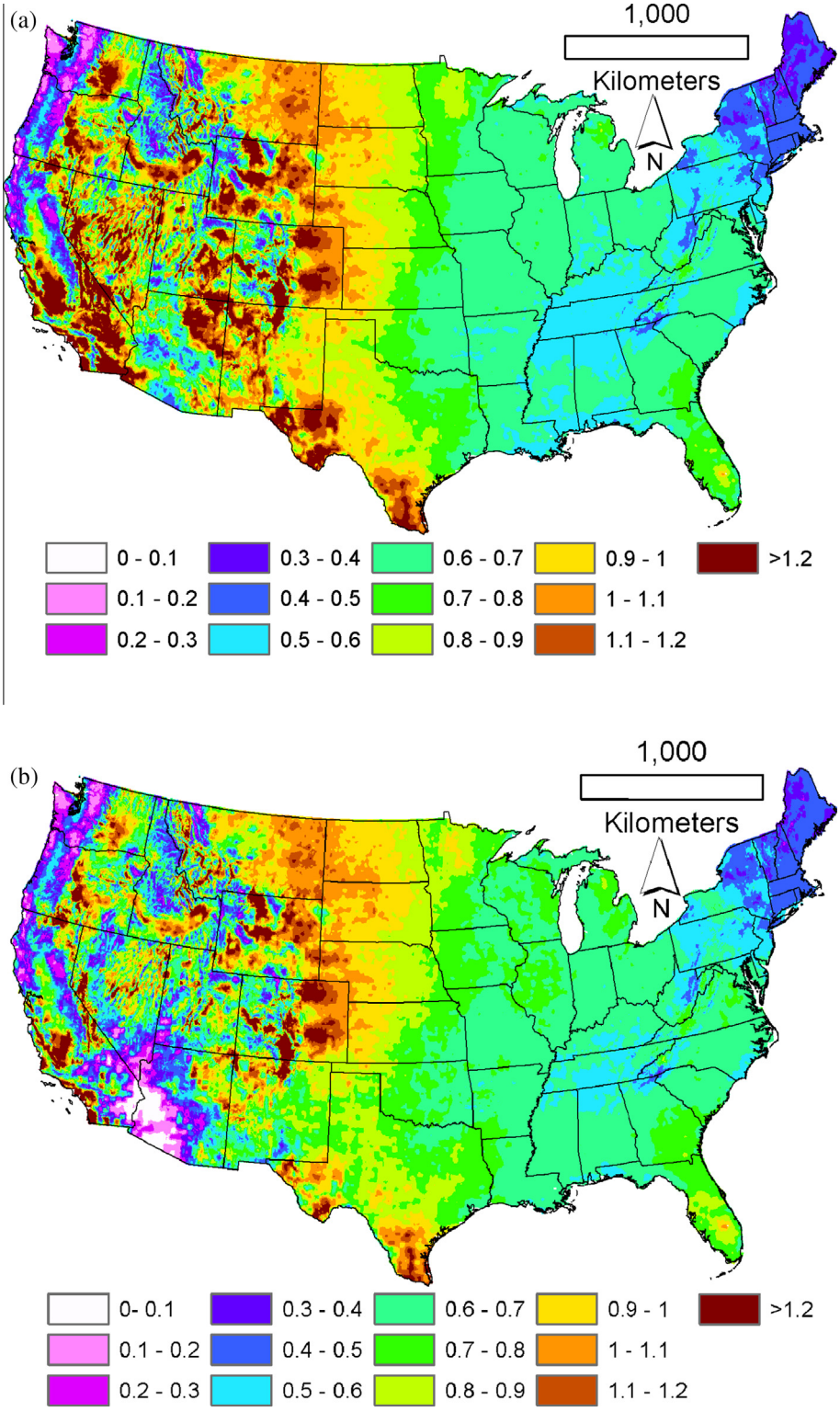

Fig. 4. Spatial distribution of the ratio of mean annual *ET* rates estimated by (a) (8) with $\alpha = 1.09$ and $c = 2$ and PRISM P ($\langle ET/P\rangle = 0.78 \pm 0.27$, $(ET/P)_{min} = 0.09$, $(ET/P)_{max} = 3.77$); (b) (9) with $\alpha = 1.14$, d = 0.28, $s = 0$, and PRISM P ($\langle ET/P\rangle = 0.73 \pm 0.24$, $(ET/P)_{min} = 0.003$, $(ET/P)_{max} = 3.5$).

becomes

$$a_3 = (d - s + ds + 1)/(d-1)^3; a_2 = (2s - d^2 s - 2d^2 - 2d - ds - 2)/(d-1)^3 \quad (9b)$$

$$a_1 = (d^3 + 2d^2 s + d^2 + 4d - s - ds)/(d-1)^3; a_0 = (ds - 2d^2 - d^2 s)/(d-1)^3 \quad (9c)$$

Constraints (a) and (b) above restrict the admissible values of the parameters to $0 \leqslant d < 1$ and $0 \leqslant s \leqslant (2d + 1)/(1 - d)$. Note that (9) is valid for $x \geqslant d$; when $x < d$, $y = 0$ is expected. Solution (9) with $d = s = 0$ yields (8) of Brutsaert (2015) with $c = 0$. (8) and (9) are intended to replace (6). Adjustment of the CR, based on the humidity of the air, as was done by Szilagyi (2015), is no longer needed.

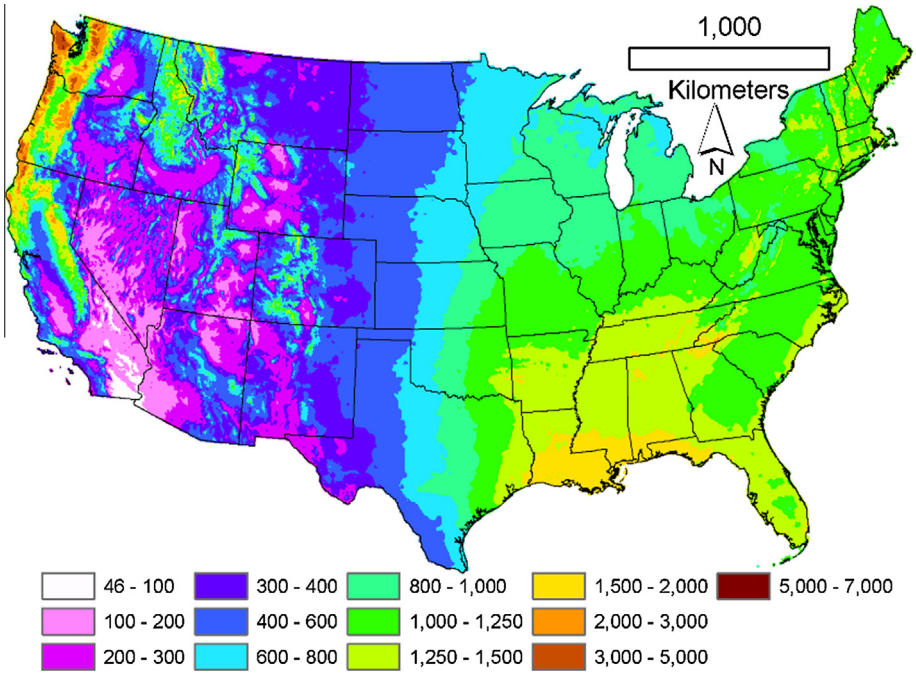

Fig. 5. Spatial distribution of mean annual (1981–2010) PRISM precipitation, $\langle P \rangle = 791 \pm 448$, $P_{min} = 47$, $P_{max} = 5984$, all in mm yr^{-1}.

Fig. 1 displays the two solutions, (8) and (9), for selected values of the parameters, c, d, and s.

The predicted CR relationships for the scaled variables are displayed in Fig. 2 as function of the moisture index, ET/E_p. Note that the $d = s = 0$ choice results in the black curves of the $c = 0$ case.

3.2. Testing the two versions of the GCR

In order to see how the GCR solution of Brutsaert (2015) and its revised version perform with measured data, (8) and (9) employing (1), (3), and (5) are applied to estimate long-term (1981–2010) mean monthly ET rates across the contiguous United States. The North American Regional Reanalysis (NARR, Mesinger et al., 2006) radiation and 10-m wind (u_{10}) as well as Parameter-Elevation Regressions on Independent Slopes Model (PRISM) precipitation, air and dew-point temperature, T_d (K), data (Daly et al., 1994) at a spatial resolution of 4 km served as data input. Note that $e(T_a) = e^*(T_d)$ for which the monthly mean PRISM T_d values are only available as 30-year normals therefore the ensuing ET estimation could not be performed on a continuous month-by-month basis, but rather as 30-year normals using similar averages of the input variables. Monthly u_{10} values were transformed to u_2 via $u_2 = u_{10}\,(2/10)^{1/7}$ (Brutsaert, 1982). Note also that BC (iii) favors the more sensitive wind function, (5), over (4) and that PRISM is widely considered to be the most accurate gridded precipitation data for the contiguous US (Daly et al., 2008). This explains the use of PRISM over NARR to obtain P.

Calibration of the parameters $-\alpha$ in (1), c in (8), and d, s in (9) – were performed by a systematic trial-and-error approach which entails trying out all possible combinations of the parameter values within predefined ranges $[1 \leqslant \alpha \leqslant 1.32,\ -1 \leqslant c \leqslant 2,\ 0 \leqslant d < 1,\ 0 \leqslant s \leqslant (2d + 1)/(1 - d)]$ set apart by similarly predefined small increments. The objective function of calibration consisted of minimizing the following two quantities for the grid-point mean annual values (Szilagyi, 2015): (a) the number of cells with $ET > P$, and; (b) the number of cells with $ET = 0$, while; (c) keeping the resulting sample mean of grid point ET values over 522 mm yr^{-1}, obtained previously by Szilagyi (2015) from (a) and (b) only. That is, ET must be within 3% of the water-balance derived sample mean of 537 mm yr^{-1}. Condition (c) was necessary because the GCR, unlike the CR version of Szilagyi (2015), kept grid point ET values above zero even with unrealistically low ET sample means. Notice that no other information was used for the calibration which itself would not prevent the resulting grid point ET rates to exceed P, as in reality $ET > P$ may occur at a mean annual basis and regional scales over lakes, marshlands and even heavily irrigated areas (Szilagyi, 2013, 2014b), it only aims to limit them to regions where it indeed happens.

4. Results

4.1. Calibration

Fig. 3 display the spatial distribution of the calibrated mean annual ET rates.

Clearly, (9) results in a wider ET range with roughly the same sample mean as (8). The number of cells with zero mean annual ET rate estimates is zero for both models while the number of cells in exceedance of PRISM precipitation (Fig. 4) is 85,298 (18% of the total number of 481,631 grid points) for (8) and 56,344 (12% of total) for (9). Large clusters of ET rates with overestimations exceeding 20% of P are predominantly found in basins and valleys of the Rocky Mountains with the most obvious exception in eastern Colorado and western Nebraska where at least some of it (especially along the Platte River in Nebraska, Colorado and Wyoming) can be explained by intensive large-scale irrigation systems (Szilagyi, 2013, 2014b).

As seen, (9) more dynamically responds to wide changes in moisture availability within the varied topography of the Rockies (the number of cells with $ET > P$ being substantially smaller) than (8), predicting small ET/P values in the mountains due to orography-enhanced precipitation (Fig. 5) and topography-boosted runoff accompanied by colder temperatures, and quite the opposite in basins with depressed precipitation and runoff rates and higher temperatures, frequently associated with large-scale irrigation schemes, a prime example being the San Luis Valley

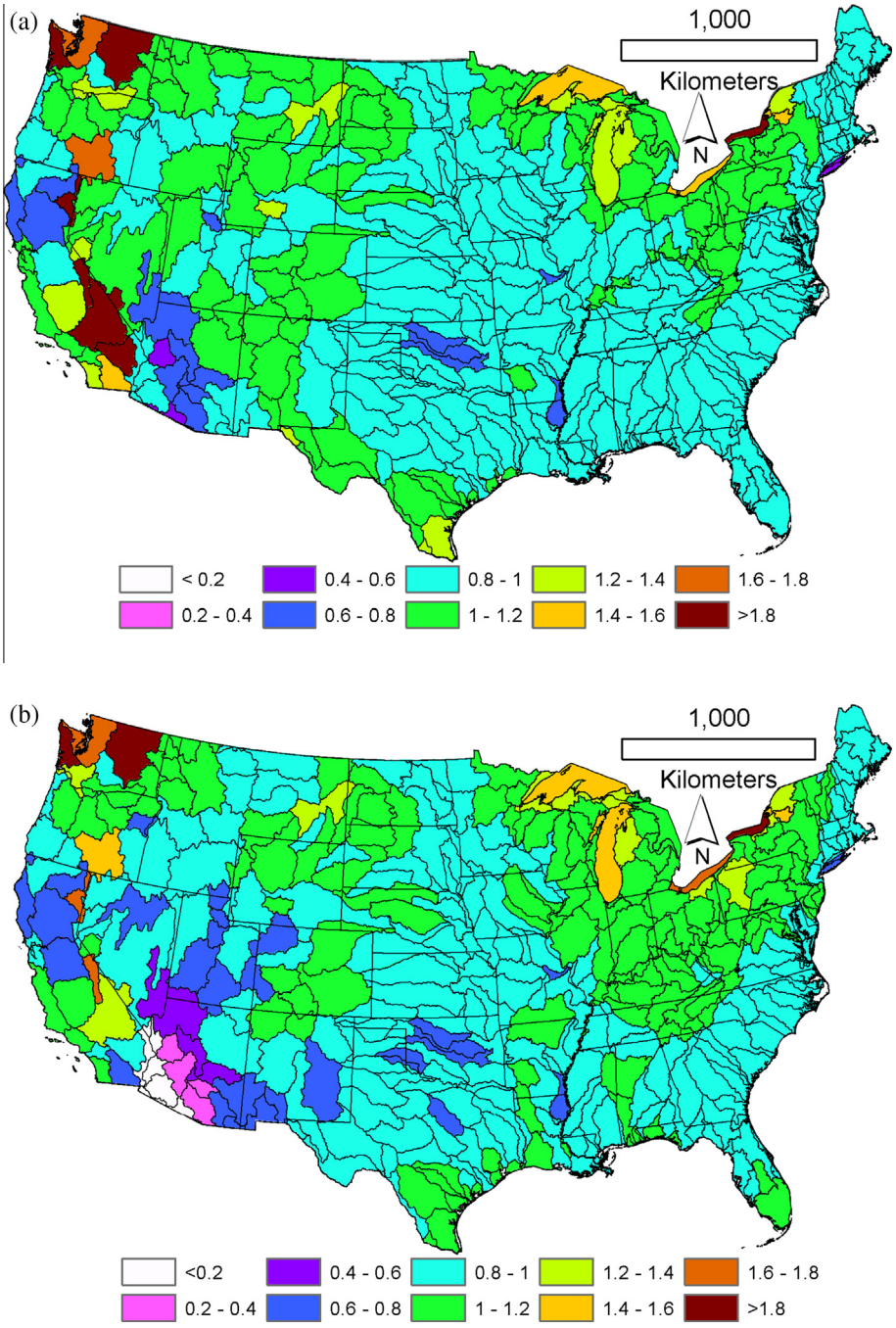

Fig. 6. Spatial distribution of the ratio of HUC6-level watershed averaged ET rates by (a) (8) and the water balance derived values as the difference of precipitation and runoff; (b) (9) and the water balance derived values.

of southern Colorado (about 300 km east of the Four-Corners Point shared by Arizona, Colorado, New Mexico and Utah in Fig. 4). An important difference can however be found in the two model versions in southern California and south-western Arizona where (8) routinely yields *ET* rates in excess of *P* while (9) undershoots since a smaller than 10% precipitation recycling ratio is probably unrealistic.

4.2. Validation

Long-term water-balance based validation of the *ET* estimates could be performed with the help of the United States Geological Survey's 6-level Hydrologic Unit Code (HUC6) runoff, *Q* (mm yr^{-1}) data (source: waterwatch.usgs.gov). For the 334 HUC6 catchments covering the conterminous US, the water-balance derived *ET* (ET_{wb}) was obtained as the difference of watershed averaged *P* (mm yr^{-1}) and *Q*. The 30-year period is long enough so that the in- and outgoing cumulative fluxes (i.e., *P* and *Q*) over the individual watersheds are much larger than any possible random annual change in water storage within the catchments. Non-random storage changes that may come from e.g., ground-water mining for intensive irrigation schemes, are accounted for in the water-balance derived *ET* rates via the resulting reduced runoff value (*Q*) as long as there is good communication between the ground- and surface-water compartments, i.e., the former collects to groundwater-fed gaining streams.

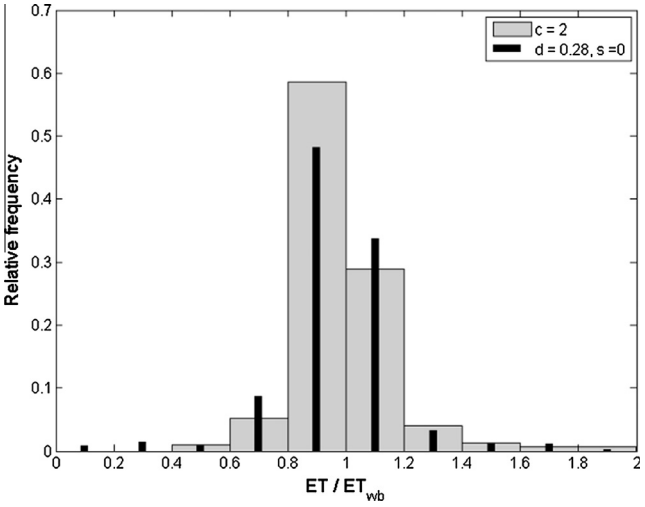

Fig. 7. Relative histograms of the HUC6-level ET/ET_{wb} ratios, $n = 334$.

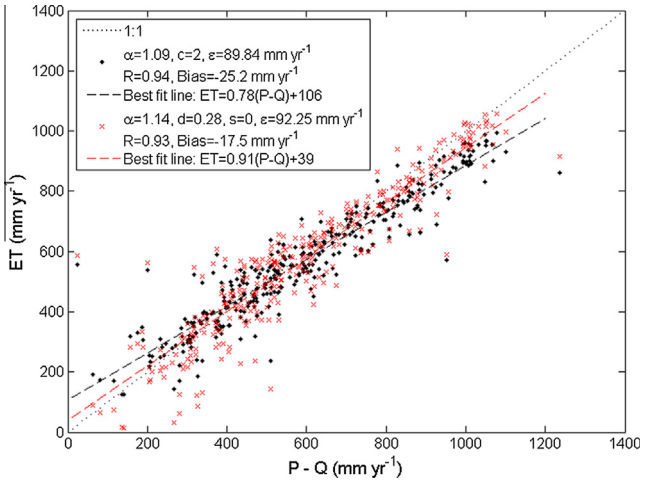

Fig. 8. Water-balance derived ($P - Q$) and theory-predicted long-term (1981–2010) mean annual ET rates for the 334 HUC6-level catchments of the contiguous US. R is the linear correlation coefficient, ε the root-mean-square error.

The spatial distribution of the ratios of HUC6-level watershed-averaged ET using (8) and (9), and water-balance derived ET rates, can be seen in Fig. 6. The results are summarized in Fig. 7 as histograms.

5. Discussion

(8) tends to underestimate water-balance ET in most catchments, although occasionally it seriously overestimates it, mostly in California and the state of Washington (dark-brown color in Fig. 6a). (9) yields a somewhat more balanced estimate with fewer major overestimations, however, it prominently underestimates catchment-wide ET rates in south-western Arizona (white patch in Fig. 6b).

A regression plot of the estimated and water-balance derived ET rates is found in Fig. 8 for the HUC6-level watersheds. The scatter of data points is somewhat smaller for (8) resulting in a better linear correlation coefficient (R) value of 0.94 vs 0.93 for (9), and a smaller root-mean-square error (ε) of about 90 vs 92 mm yr^{-1} for (9). At the same time (8) more seriously underestimates ET_{wb} than (9) at large values, reflected in a larger bias and a flatter best fit line.

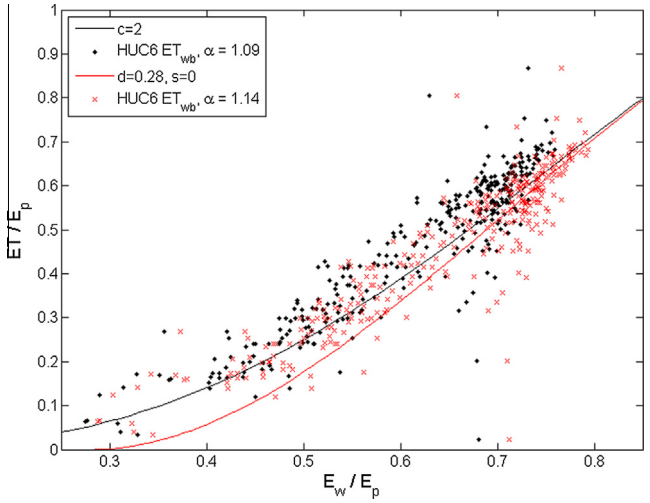

Fig. 9. E_p-scaled water-balance derived (ET_{wb}) and theory-predicted long-term (1981–2010) mean annual ET rates for the 334 HUC6-level catchments as function of the scaled wet-environment evaporation rates. The water-balance derived points occur at horizontally shifted positions due to different calibrated values of α for (8) and (9).

When the theory-predicted scaled ET rates are compared with similarly scaled water-balance ET values plotted against $x = E_w/E_p$, the typical underestimation of (8) is more obvious at almost all values of x, while (9) better fits ET_{wb} rates at larger x values (Fig. 9). Also, the steeper slope of (9) at low x values makes it more sensitive to moisture availability in drier environments leading to a significantly smaller number of overestimated grid point ET rates in excess of precipitation (Fig. 4).

From the relevant model parameters, both models are most sensitive to the value of α (Fig. 10), so it must be calibrated the most accurately.

6. Summary and discussion

The recently developed generalized complementary relationship of Brutsaert (2015) and its revised version have been tested with HUC6-level catchment runoff data covering the contiguous United States. The revised version, (9), with its two free parameters performed better than the one-parameter solution, (8), in its (a) dynamic response to moisture availability changes over relatively short distances [occurrence, $f_{(ET>P)}$, of ET rates in excess of P is 12% of total grid-points vs 18% of (8)]; (b) mean bias of the estimates (-17 vs -25 mm yr^{-1}); and c) slope of the best-fit regression line ($m = 0.91$ vs 0.78). At the same time, (8) resulted in a higher linear correlation coefficient value [$R = 0.94$ vs 0.93 of (9)] and a smaller root-mean-square error ($\varepsilon = 90$ vs 92 mm yr^{-1}). Calibration has been performed with PRISM precipitation rather than HUC6-derived water balance data in order to (a) separate calibration from validation by using different data sets, which thus is expected to lead to a more robust model performance, and; (b) coerce as much dynamics from the model as possible by ensuring that it effectively responds to quick changes in moisture availability within short distances over, e.g., the varied topography of the Rockies, and not only to some spatially-averaged moisture availability measure obtainable at the watershed scale.

The recent GCR-based model versions perform about the same [(9) perhaps slightly better] as the modified CR model of Szilagyi (2015) which introduced a two-parameter aridity-based scaling function for b^{-1} of (6) and was calibrated and validated ($f_{(ET>P)} = 12\%$, $m = 0.89$, Bias $= -18$ mm yr^{-1}, $R = 0.92$, $\varepsilon = 96$ mm yr^{-1}) with the recent data sets.

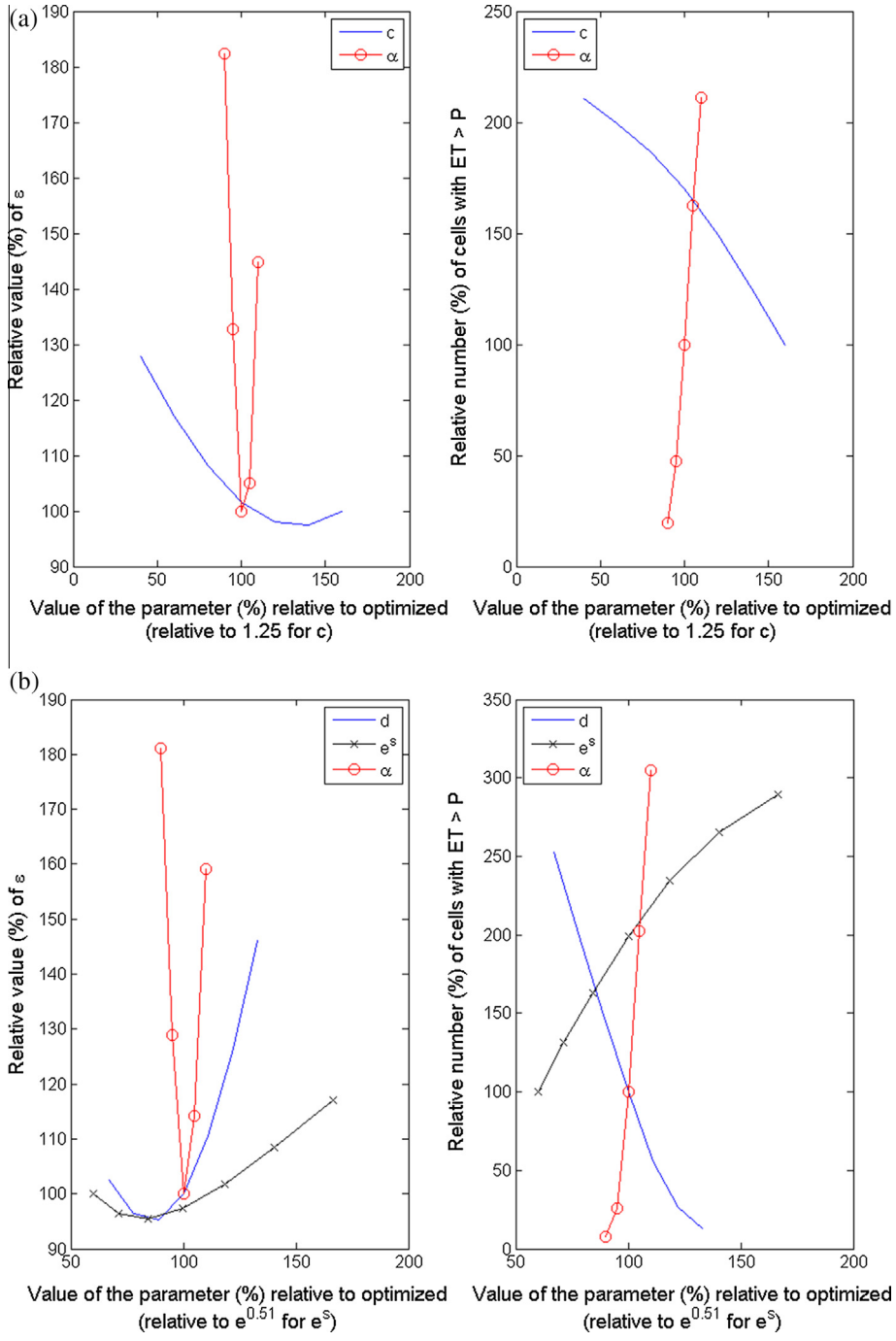

Fig. 10. Sensitivity of selected model performance to changes in parameter values (a) c and α of (8) (values of c are compared to a smaller, non-optimal value for obtaining a range similar to that of α); (b) d, s, and α of (9). ε is the root-mean-square error. Exponentials are taken for s because of its zero optimized value and compared to a larger, non-optimal value for obtaining a range similar to those of the other parameters.

Future improvements in *ET* estimation by the CR-based models could be achieved via improving the spatial resolution of the radiation input data which causes a grainy structure especially in Fig. 3, even after some edge-smoothing filtering. A finer resolution radiation dataset could also account for slopes, their orientation and the shading effect of the surrounding mountain slopes and thus could be expected to significantly improve dynamic *ET* response over short distances. A word of caution for potential CR-based *ET* estimation model users: there is an inherent limit for spatial resolution of such approaches. It comes from the central assumption of the method, which is that the moisture content of the air is the result of the moisture availability of the surrounding landscape. Near the border of sudden discontinuities in moisture availability of the surface (such as sea/lake shores, the boundary of extensive, heavily irrigated areas especially in arid environments) the moisture content of the air may be severely decoupled from that of the surrounding land (Morton, 1983). Based on available data (Davenport and Hudson, 1967; Lang et al., 1974) the typical horizontal scale-length of such a transition zone is in the order of 10^2–10^3 m, which thus forms the limit for the highest possible spatial resolution of the CR-based *ET* estimation approaches, which does not seem utterly restrictive considering the current relatively coarse spatial resolution of generally available large-scale radiation data.

7. Conclusion

All CR-based methods consider the complex interplay between soil moisture, vegetation, evapotranspiration and water vapor content of the air and derives the corresponding *ET* rate from standard meteorological measurements only, without the need of information on the interacting land-soil-vegetation components, other methods, such as Land Surface Models (LSM), require. LSMs provide sensible and latent heat fluxes typically employing variations of the Penman–Monteith equation (Monteith, 1965) for the latter, requiring soil and vegetation information to perform soil moisture budgeting. Considering the typically large heterogeneity in soil type, thickness, layering, vegetation-cover and rooting depth, the ensuing *ET* fluxes may contain relatively high uncertainties, resulting in noticeable differences in *ET* values among LSM versions (Sheffield et al., 2012), giving rise to the need for an alternative formulation of the *ET* fluxes not requiring such information, as was demonstrated here.

Acknowledgments

The authors are grateful to the reviewers and Editor for their valuable comments that greatly improved the original manuscript.

References

Bouchet, R.J., 1963. Evapotranspiration reelle, evapotranspiration potentielle, et production agricole. Ann. Agron. 14, 743–824.
Brutsaert, W., 1982. Evaporation into the Atmosphere: Theory, History and Applications. D. Reider, Dordrecht, Holland, p. 299.
Brutsaert, W., 2005. Hydrology: An Introduction. Univ. Cambridge Press, Cambridge, UK, p. 605.
Brutsaert, W., 2015. A generalized complementary principle with physical constraints for land-surface evaporation. Water Resour. Res. 51. http://dx.doi.org/10.1002/2015WR017720.
Brutsaert, W., Stricker, H., 1979. An advection-aridity approach to estimate actual regional evapotranspiration. Water Resour. Res. 15, 443–449.
Culf, A.D., 1994. Equilibrium evaporation beneath a growing convective boundary layer. Bound. Layer Meteorol. 70, 37–49.
Daly, C., Neilson, R.P., Phillips, D.L., 1994. A statistical topographic model for mapping climatological precipitation over mountainous terrain. J. Appl. Meteorol. 33, 140–158.
Daly, C., Halbleib, M., Smith, J.I., Gibson, W.P., Doggett, M.K., Taylor, G.H., Curtis, J., Pasteris, P.P., 2008. Physiographically sensitive mapping of climatological temperature and precipitation across the conterminous United States. Int. J. Clim. 28 (15), 2031–2064. http://dx.doi.org/10.1002/joc.1688.
Davenport, D.C., Hudson, J.P., 1967. Changes in evaporation rates along a 17-km transect in the Sudan Gezira. Agric. Meteorol. 4, 339–352.
de Bruin, H.A.R., 1983. A model for the Priestley-Taylor parameter α. J. Clim. Appl. Meteorol. 22, 572–580.
Heerwaarden, C.C., Arellano, J.V., Moene, A.F., Holtslag, A.A.M., 2009. Interactions between dry-air entrainment, surface evaporation and convective boundary-layer development. Quart. J. Roy. Meteorol. Soc. 135, 1277–1291.
Han, S., Hu, H., Tian, F., 2012. A nonlinear function approach for the normalized relationship evaporation model. Hydrol. Process. 26, 3973–3981. http://dx.doi.org/10.1002/hyp.8414.
Huntington, J., Szilagyi, J., Tyler, S., Pohll, G., 2011. Evaluating the complementary relationship for estimating evapotranspiration from arid shrublands. Water Resour. Res. 47, W05533. http://dx.doi.org/10.1029/2010WR009874.
Kahler, D.M., Brutsaert, W., 2006. Complementary relationship between daily evaporation in the environment and pan evaporation. Water Resour. Res. 42, W05413. http://dx.doi.org/10.1029/2005WR 004541.
Lang, A.R.G., Evans, G.N., Ho, P.Y., 1974. The influence of local advection on evapotranspiration from irrigated rice from a semi-arid region. Agric. Meteorol. 13, 5–13.
Lhomme, J.P., 1997. A theoretical basis for the Priestley-Taylor coefficient. Bound. Layer Meteorol. 82, 179–191.
McMahon, T.A., Peel, M.C., Lowe, L., Srikanthan, R., McVicar, T.R., 2013a. Estimating actual, potential, reference crop and pan evaporation using standard meteorological data: a pragmatic synthesis. Hydrol. Earth Syst. Sci. 17, 1331–1363. http://dx.doi.org/10.5194/hess-17-1331-2013.
McMahon, T.A., Peel, M.C., Szilagyi, J., 2013b. Comment on the application of the Szilagyi-Jozsa advection–aridity model for estimating actual terrestrial evapotranspiration in "Estimating actual, potential, reference crop and pan evaporation using standard meteorological data: a pragmatic synthesis" by McMahon et al. (2013). Hydrol. Earth Syst. Sci. 17, 4865–4867. http://dx.doi.org/10.5194/hess-17-4865-2013.
Mesinger, F., DiMego, G., Kalnay, E., Mitchell, K., Shafran, P.C., Ebisuzaki, W., Jović, D., Woollen, J., Rogers, E., Berbery, E.H., Ek, M.B., Fan, Y., Grumbine, R., Higgins, W., Li, H., Lin, Y., Manikin, G., Parrish, D., Shi, W., 2006. North American regional reanalysis. Bull. Am. Meteorol. Soc. 87, 343–360.
Monteith, J.L., 1965. Evaporation and environment. The State and Movement of Water in Living Organisms. In: Fogg, G.E. (Ed.), Symposium of the Society of Experimental Biology, vol. 19. Cambridge University Press, pp. 205–234.
Morton, F.I., 1983. Operational estimates of areal evapotranspiration and their significance to the science and practice of hydrology. J. Hydrol. 66, 1–76.
Penman, H.L., 1948. Natural evaporation from open water, bare soil, and grass. Proc. Roy. Soc. Lond. A193, 120–146.
Priestley, C.H.B., Taylor, R.J., 1972. On the assessment of surface heat flux and evaporation using large-scale parameters. Mon. Weather Rev. 100 (2), 81–92.
Ramirez, J.A., Hobbins, M.T., Brown, T.C., 2005. Observational evidence of the complementary relationship in regional evaporation lends strong support for Bouchet's hypothesis. Geophys. Res. Lett. 32, L15401. http://dx.doi.org/10.1029/2005GL023549.
Sheffield, J., Livneh, B., Wood, E.F., 2012. Representation of terrestrial hydrology and large-scale drought of the continental United States from the North American Regional Reanalysis. J. Hydrometeor. 13, 856–876. http://dx.doi.org/10.1175/JHM-D-11-065.1.
Szilagyi, J., 2007. On the inherent asymmetric nature of the complementary relationship of evaporation. Geophys. Res. Lett. 34, L02405.
Szilagyi, J., 2013. Recent updates of the Calibration-Free Evapotranspiration Mapping (CREMAP) method. In: Alexandris, S. (Ed.), Evapotranspiration – An Overview. INTECH, Rijeka, Croatia, ISBN 980-953-307-541-4. <http://www.intechopen.com/books/evapotranspiration-an-overview>.
Szilagyi, J., 2014a. Temperature corrections in the Priestley-Taylor equation of evaporation. J. Hydrol. 519, 455–464. http://dx.doi.org/10.1016/j.jhydrol.2014.07.040.
Szilagyi, J., 2014b. MODIS-aided water-balance investigations in the Republican River basin, USA. Periodica Polytech. Civ. Eng. 58 (1), 33–46.
Szilagyi, J., 2015. Complementary-relationship-based 30 year normals (1981–2010) of monthly latent heat fluxes across the contiguous United States. Water Resour. Res. 51, 9367–9377. http://dx.doi.org/10.1002/2015WR017693.
Szilagyi, J., Jozsa, J., 2008. New findings about the complementary relationship-based evaporation estimation methods. J. Hydrol. 354 (1–4), 171–186.
Szilagyi, J., Jozsa, J., 2009. Analytical solution of the coupled 2-D turbulent heat and vapor transport equations and the complementary relationship of evaporation. J. Hydrol. 372, 61–67.
Szilagyi, J., Schepers, A., 2014. Coupled heat and vapor transport: the thermostat effect of a freely evaporating land surface. Geophys. Res. Lett. 41 (2), 435–441. http://dx.doi.org/10.1002/2013GL 058979.
Zuo, H., Chen, B., Wang, S., Guo, Y., Zuo, B., Wu, L., Gao, X., 2015. Observational study on complementary relationship between pan evaporation and actual evapotranspiration and its variation with pan type. Agric. Forest Meteorol. 222, 1–9. http://dx.doi.org/10.1016/j.agrformet.2016.03.002.